

Simulating precursor steps for fibril formation in methylcellulose solutions

Vaidyanathan Sethuraman and Kevin D. Dorfman*

*Department of Chemical Engineering and Materials Science, University of Minnesota–Twin Cities,
421 Washington Ave. SE, Minneapolis, Minnesota 55455, USA*



(Received 17 March 2019; published 1 May 2019)

We use coarse-grained molecular dynamics simulations to study the precursor steps for fibril formation in methylcellulose solutions. Simulations of ring stacking between two collapsed methylcellulose chains demonstrate the existence of a capture radius that is much larger than that predicted by polymer diffusion alone. When two rings are in very close proximity, they stack together to form a fibril precursor. Simulations of stacks of such rings suggest that this structure is metastable. In contrast, chains that are within the capture radius but not in close proximity, as well as for systems containing both ringlike and relaxed chains, fibril-like structures form via a distinctly different mechanism. Irrespective of their initial arrangement, the chains undergo two specific conformational changes: (i) a part of either a ring or a randomly coiled chain splays out and (ii) the splayed chain subsequently engulfs a nearby chain if it is within a certain capture distance. The latter results are consistent with recent experimental measurements of fibril formation by short methylcellulose chains, which suggests the formation of a twisted bundle.

DOI: [10.1103/PhysRevMaterials.3.055601](https://doi.org/10.1103/PhysRevMaterials.3.055601)

I. INTRODUCTION

Methylcellulose (MC) is a cellulose-based ring polymer with one to three hydroxyl groups replaced by methyl groups at the C-2, C-3, and/or C-6 positions. The degree of substitution (DS) quantifies the number of methyl substitutions per MC monomer and varies between zero and three. Commercially available MC, known as METHOCEL A, is a random copolymer with an average DS of 1.80 and is soluble in water at room temperature. Such aqueous MC solutions exhibit lower critical solution temperature (LCST) behavior, forming stable hydrogels comprised of fibrils [1–3] at high temperatures (above 50 °C) [3]. Although MC has been a subject of research since the early 1900s [4–12], there has been a renewed interest in the phase behavior [1,13–17], conformational properties [2,3,18–26], and mechanical properties [3,25,27,28] of MC polymers. While these experimental and computational efforts provided significant insights into the final fibril structure, the mechanism leading up to fibril formation remains poorly understood.

The renewed interest in methylcellulose initiated with the work of Lott *et al.* [1], where they utilized small-angle neutron scattering to show that methylcellulose aggregates in solution at very low concentrations to form fibrils of uniform diameter of 14 ± 1 nm at elevated temperatures (70 °C). They also showed that the fibrils contained about 40% polymer. A preliminary conjecture for these observations was that the fibrils consisted of stacked chains with a water-filled core. To understand the equilibrium phase diagram for these systems, Larson and co-workers used a coarse-grained model for an isolated semiflexible chain with attractive backbone interactions and showed that they can adopt toroidal, bundled, or globular

shapes depending upon the competition between bead-bead attraction strength and backbone stiffness [29]. Subsequently, based on this idea, they developed a coarse-grained model for methylcellulose [18] and showed that isolated methylcellulose chains collapse into rings at high temperatures. However, the precursor mechanism for fibril formation in methylcellulose was unexplored.

In an effort to model the precursor steps for fibril formation, Ginzburg *et al.* used coarse-grained simulations of systems containing two to fifteen MC chains [30] using the coarse-grained model developed by Larson and co-workers [18]. They proposed that, upon heating, the randomly coiled MC chains at low temperature collapse to form toroids with a uniform outer diameter of 13.9 ± 0.4 nm, consistent with experimental observations [1]. They further proposed that these ring-shaped molecules then stack on top of each other to form fibrils with a water-filled core. The results of these simulations, while providing a plausible mechanism for fibril formation, contrast with a recent experimental study on MC fibril formation over a large spectrum of molecular weights, where cryo-TEM measurements suggest the formation of a twisted bundle [26]. Importantly, low molecular weight MC produced shorter fibrils, suggesting that the MC chains bundle helically around a “core” chain with water distributed throughout the radial dimension. However, in the absence of finer experimental resolution, this conjecture could not be verified.

Motivated by the differences between simulations and experiments pertaining to the mechanism of fibril formation, we extend the current understanding of MC fibril formation using coarse-grained simulations that go beyond the conditions explored previously [30]. To this end, we take advantage of the coarse-grained model developed by Larson and co-workers [18] that was used in the aforementioned simulations of ring stacking [30]. Long MD simulations were performed

*dorfman@umn.edu

for a number of model systems to determine the intermediate steps leading to fibril formation. Our simulations show the mechanism of fibril formation depends strongly upon the initial separation between the chains, and that spontaneous fluctuations of the chain conformations play a significant role in guiding fibril formation.

II. METHODOLOGY

A. Simulation details

We employed coarse-grained molecular dynamics to analyze the conformations of methylcellulose in solution. All MC chains were modeled as heterogenous random copolymers with all possible combinations of DS. The bead identities, distinguished by their DS, were chosen at random with an average DS of each polymer chain being 1.80 [18]. The solvent molecules were implicit. Simulations were performed using the LAMMPS [31] package for a total of at least 2.0×10^7 time steps (inclusive of both equilibration and production cycles) for systems containing more than two chains. The total simulation times for systems containing two chains were at least 8×10^6 steps. The time step varied between 3×10^{-4} and $5 \times 10^{-4} \tau$ (unless otherwise mentioned), where τ is the time in LJ units and corresponds to approximately 0.028 ns [18]. All simulations were performed at a reduced temperature of 1.0 in LJ units.

Details on interaction potentials and potential parameters, which correspond to the model of Huang *et al.* [18], are recapitulated in Sec. S1 of the Supplemental Material [32]. Our simulations entailed three minor modifications to this coarse-grained model. (i) The masses of all monomeric units were scaled to the mass of monomeric unit of a MC with a degree of substitution $DS = 0$. Previous works utilized the same mass (unity) for all monomeric units, irrespective of the DS. (ii) We evolved the system in a NVT ensemble using N ose-Hoover thermostat, rather than the Langevin thermostat [33] utilized in the aforementioned work. (iii) 1–5 interactions were absent in our model. The first change should provide better correspondence with experiments, since the molecular weights of monomers with different DS vary slightly. The second change ensures that the system conserves the Hamiltonian in the canonical ensemble. Systems evolved in the presence of a Langevin thermostat exhibit large fluctuations in temperature and correspondingly large fluctuations in radius of gyration of the molecule—particularly at the low molecular weights used here (Fig. S2 [32]). Finally, although the last assumption may create small changes in the long-range interactions, previous work by Li *et al.* [19] showed that the qualitative results are insensitive to the absence of 1–5 interactions. In Sec. III A, we test the implication of the trio of assumptions by comparing two-chain simulations of proximate rings to previous work by Ginzburg *et al.* [30].

B. Systems studied

We simulated two-chain systems initialized in ringlike configurations and multichain systems (greater than two chains) in different initial configurations. Multichain systems corresponded to the following initial arrangements: (i) the block configuration in Fig. 1(a), wherein the chains in ring

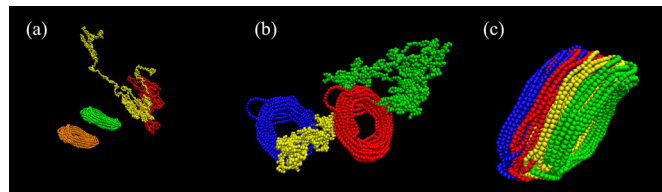


FIG. 1. Representative initial conditions for (a) block, (b) alternating, and (c) jammed initial configuration.

configuration were stacked near each other and followed by a set of randomly coiled chains, (ii) the alternating configuration in Fig. 1(b), wherein the chains alternated between an initial ring configuration and initial random configuration, and (iii) the jammed configuration in Fig. 1(c), wherein multiple rings were stacked very close to each other. The choice of these initial configurations allows us to elucidate cleanly the steps leading to the transformation of randomly coiled chains into a ring conformation in the presence of other ring chains, and the conformational changes occurring after the fibril-like structure is formed. The algorithms for generating the initial configurations are provided in Sec. S2 [32].

C. Quantification measures

1. Shape anisotropy factor of individual polymer chains

The gyration tensor [34] of the i th chain is defined using the second moment of the monomer positions of that polymer chain,

$$S_{mn}^i = \frac{1}{N} \sum_j r_m^j r_n^j, \quad (1)$$

where r_m^j represents the m th Cartesian coordinate ($m \in \{x, y, z\}$) of the j th monomer and N represents the degree of polymerization of the i th chain. The reference frame for the tensor is chosen such that the centroid coordinate of the i th chain is subtracted from all the monomer positions before the gyration tensor is computed. The radius of gyration tensor can then be diagonalized to obtain three squared eigenvalues ($\{\lambda_x^2, \lambda_y^2, \lambda_z^2\}$). The eigenvalues are arranged in such a way that $\lambda_z^2 \geq \lambda_y^2 \geq \lambda_x^2$. Large changes in any eigenvalue correspond to large changes in the structure of that chain at that time instant.

The squared eigenvalues can then be utilized to compute the shape anisotropy factor of the i th chain,

$$\kappa_i^2 = 1 - 3 \frac{(\lambda_x^2 \lambda_y^2 + \lambda_x^2 \lambda_z^2 + \lambda_y^2 \lambda_z^2)}{(\lambda_x^2 + \lambda_y^2 + \lambda_z^2)^2}. \quad (2)$$

The values of $\kappa_i^2 = 0, 0.25,$ and 1.0 correspond to a straight line, ring, and sphere, respectively. For cases where the shape anisotropy does not change much during the course of the simulation, it is convenient to define the difference in shape anisotropy factor

$$\Delta \kappa_i^2 = \kappa_i^2(t) - \kappa_i^2(t=0), \quad (3)$$

where $\kappa_i^2(t)$ is the shape anisotropy factor of the i th chain at time t and $\kappa_i^2(t=0)$ is the shape anisotropy factor of the same chain at the beginning of the simulation.

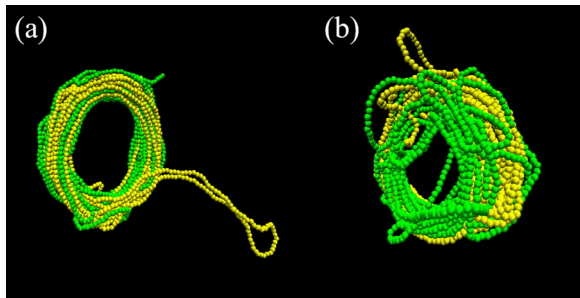


FIG. 2. Final structures of two-chain systems with the initial distance between their centers of mass r_0 being (a) 3σ and (b) 8σ .

2. Global shape anisotropy factor

To understand the shape of the overall fibril structure, we compute the global shape anisotropy factor (κ_g^2). The global centroid $\mathbf{r}_{\text{cm},g}$ for computing κ_g^2 is computed as

$$\mathbf{r}_{\text{cm},g} = \frac{1}{Nn} \sum_i^{Nn} \mathbf{r}^i, \quad (4)$$

where N and n denote the degree of polymerization of the chain and the number of chains within the system. The global gyration tensor S_{mn}^g is computed using

$$S_{mn}^g = \frac{1}{Nn} \sum_i^{Nn} r_m^i r_n^i, \quad (5)$$

where r_m^i is measured relative to $\mathbf{r}_{\text{cm},g}$. The eigenvalues obtained from diagonalizing the global radius of gyration tensor [Eq. (5)] are then used to compute the global shape anisotropy factor using Eq. (2).

III. RESULTS AND DISCUSSION

A. Fibril formation in systems of collapsed rings

To probe the influence of methylcellulose concentration, we consider simulations with two collapsed toroids with different initial distance r_0 between their centers of mass. We look first at systems comprising closely packed MC toroidal chains with r_0 between 3σ and 9σ , revisiting the cases investigated by Ginzburg *et al.* [30]. Since attractive interactions lead to quick collapse of the two chains into a single object, these simulations provide insights into the behavior of the system at high concentrations of collapsed systems even if the actual concentration (monomers per simulation volume) may not actually be high. Figure 2 displays representative final configurations of two-chain systems for two different values of r_0 at the beginning of the simulation. We repeated these simulations for four independent initial configurations, and the qualitative results were independent of the initial configuration. To avoid repetition, we present only one set of results.

When r_0 is approximately between 3σ and 9σ , we observe ring stacking in Fig. 2, confirming the results by Ginzburg *et al.* [30]. The transition between ring stacking the other types of behavior discussed later is not sharp; one should

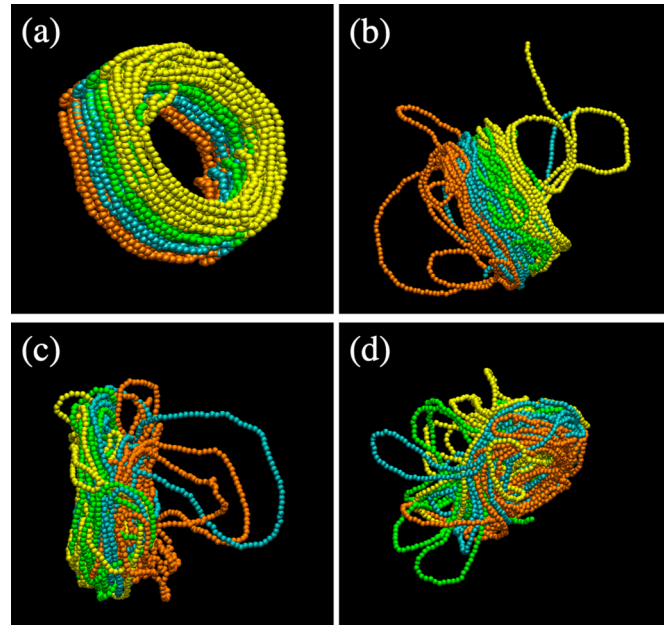


FIG. 3. Snapshots for a four-chain system initiated in a jammed configuration. Snapshots are taken at (a) 0τ , (b) 1360τ , (c) 9265τ , and (d) 13695τ .

view values such as the upper bound $r_0 = 9\sigma$ as the approximate position of the transition between behaviors. The correspondence with previous work demonstrates that the minor differences between the simulation techniques described in Sec. II A and those adopted by Ginzburg *et al.* [30] do not affect the qualitative trends in the simulation results.

Before proceeding to dilute MC solutions, it is worthwhile to probe the stability of a fibril structure produced by stacking rings. The ring stacking mechanism [30] implicitly assumes that the rings within the precursor structure are stable and that the nearby rings stack onto the ends of the precursor to form the final fibril structure. To examine this hypothesis in detail, we consider the four identical chains initially packed closely in the ring structure in Fig. 3(a). If ring stacking is the precursor to fibril formation, then, at most, only those rings at the end (color coded in brown and yellow here) within the “stable” fibril structure should undergo conformational fluctuations. However, the snapshots displayed in Fig. 3 clearly indicate that all the four chains undergo significant conformational fluctuations.

To quantify the magnitude of the conformational fluctuations and provide information throughout the course of the simulation, Fig. 4 provides the difference in the shape anisotropy factor $\Delta\kappa_i^2$ [Eq. (3)]. Changes in the difference in shape anisotropy factor can be observed for all four chains at different times, indicating that none of the chains maintain their initial ring structure. The orange and yellow chains, which correspond to the outer rings, exhibit the largest fluctuations, indicating that the probability for the inner chains to act as nucleating sites is smaller. As a result, the probability for fibril formation to proceed along the axial direction is higher than along any other direction, favoring the formation of the long fibrils [2,26]. Branching could occur during conformational fluctuations of the inner rings leading to defective

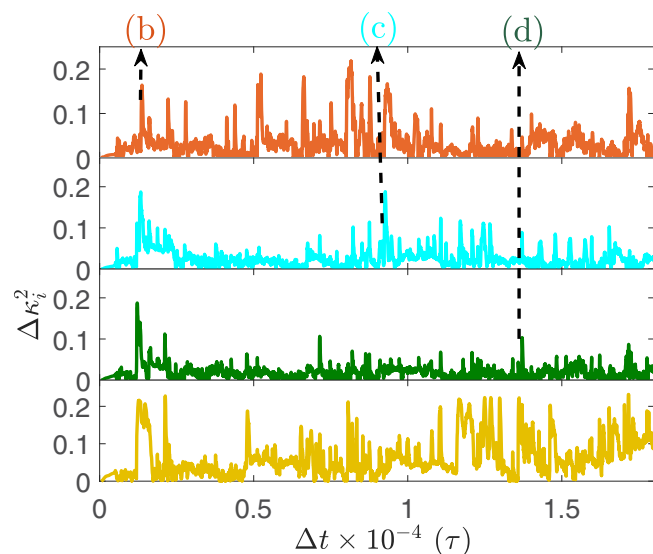


FIG. 4. Difference in the shape anisotropy factor between successive frames ($\Delta\kappa_i^2$) as a function of time for all chains for the jammed configuration. The labels for the vertical dashed lines correspond to the times of the snapshots in Fig. 3, with the text color corresponding to the particular chain referenced by the label.

fibrils. Simulations of an eight-chain system also exhibit similar trends and are shown in Fig. S3 [32].

Since experiments are conducted over a range of concentrations that are typically more dilute than those in Fig. 2, it is illuminating to examine the mechanism of fibril formation at larger initial separation distances. Figures 5(a) and 5(b) show that the rings collapse into a single fibril without defects when $r_0 \lesssim 30\sigma$ apart. However, when r_0 lies between 30σ and 40σ , different configurations emerge including defective fibrils,

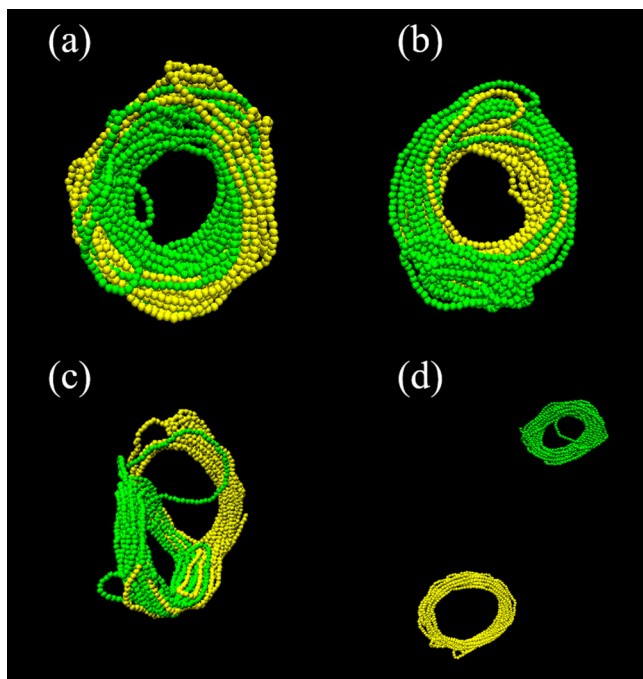


FIG. 5. Final structure of two-chain systems with $r_0 =$ (a) 13σ , (b) 18σ , (c) 36σ , and (d) 45σ .

isolated rings, and collapsed states. For instance, Fig. 5(c) shows a defective fibril at the end of the simulation. For completeness, Fig. S4 [32] displays the initial configuration and the configuration at the end of the simulation for all the simulations performed for r_0 between 30σ and 45σ . Within the duration of the simulations, two chains remain as separate entities when the initial distance between them is greater than approximately 45σ . These results suggest that when the chains are within 30σ apart, the chains tend to collapse. We call this distance the minimum capture radius for fibril formation, keeping in mind that the cutoff at 30σ is an approximate value between chain capture and diffusive escape.

A plausible hypothesis for fibril formation for isolated rings with r_0 between 9σ and 30σ is that the chains diffuse until they are proximate to one another, whereupon they stack instantly. To test the plausibility of this hypothesis in practice, we compute the diffusion time for the chains. The Stokes-Einstein diffusion coefficient (D_{SE}) obtained from experimental measurements of the hydrodynamic radius of MC chains and the viscosity of MC solutions is estimated to be $\approx 10^{-11}$ m²/s for a chain with a degree of polymerization of 1000 [18,35]. The diffusion time, τ_D , in these cases scales as r_0^2/D_{SE} . When r_0 is 15σ (8.25 nm), $\tau_D \approx 7$ μ s. However, from our simulations, two chains initially separated by 15σ collapse within approximately 0.05 μ s ($\approx 2000\tau$ [18,32]). Since the simulated time scales for chain collapse are much smaller than the diffusion time scale, we conclude that the center of mass polymer diffusion alone is not the driving mechanism for chains with these initial separation distances. Rather, conformational fluctuations in the MC chains drive the system to form fibrils when they are within these intermediate length scales, consistent with the claims by Li *et al.* [19] that conformational fluctuations play a major role in fibril formation involving multiple rings.

When $r_0 \gtrsim 45\sigma$, the chains do not collapse into a fibril within the simulation time [cf. Fig. 5(d)]. In this case, the only way the chains will find each other is through random diffusion to within the minimum capture radius, which is a very slow process compared to the conformational fluctuations. This result serves as a partial explanation for the experimental observation of extremely large time scales for fibril formation [2]. Together, these results suggest that the chains diffuse at random, and when the chains are within the capture radius, spontaneous fibril formation occurs via conformational fluctuations.

B. Fibril formation in a system of rings and randomly coiled chains

The preceding results indicate that the fibril formation mechanism depends on the initial separation distance between MC chains. However, the chains in the simulations leading us to this conclusion were initiated in a toroidal configuration. This scenario implies a two-stage fibril formation mechanism, where isolated chains first collapse into rings followed by ring stacking. It is thus worthwhile to see whether the fibril formation mechanism observed for two-chain systems holds for multichain systems consisting of both ring and random chain configurations. If the two-step process holds true, then

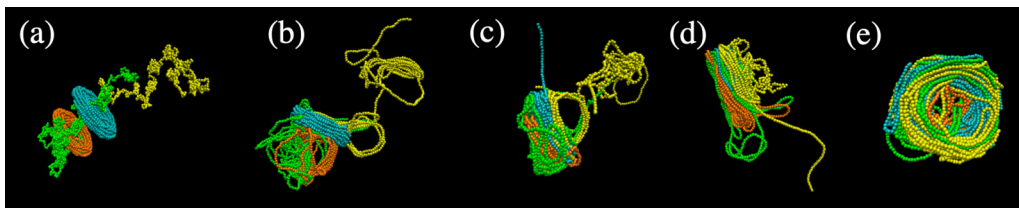


FIG. 6. Mechanism of ring formation consisting of four chains and initiated in an alternating configuration. Snapshots are taken at (i) 0τ , (ii) 880τ , (iii) 1510τ , (iv) 5095τ , and (v) 9660τ (last configuration for this simulation).

we should expect the randomly coiled chains to collapse first, and then the rings should stack into a fibril.

To this end, we consider first a system with four chains initiated in the alternating configuration shown in Fig. 6(a). The initial configuration was set up such that the centers of mass of the adjacent chains are 10σ apart, and the randomly coiled chains lie in between the rings. Figure 6 displays snapshots of the major steps of fibril formation, and Figs. 7(a) and 7(b) quantify these observations by providing individual (κ_i^2) and the global shape anisotropy factor (κ_g^2), respectively. For ease of reference to the pictorial depiction in Fig. 6, we add the corresponding figure labels in Fig. 7(a).

Our simulation data are inconsistent with a two-stage process of ring collapse and stacking. Figure 7(a) shows that two curves start around 0.2–0.25 (color coded in orange and cyan, respectively), indicating that their initial structures are ringlike and consistent with the initial configuration shown

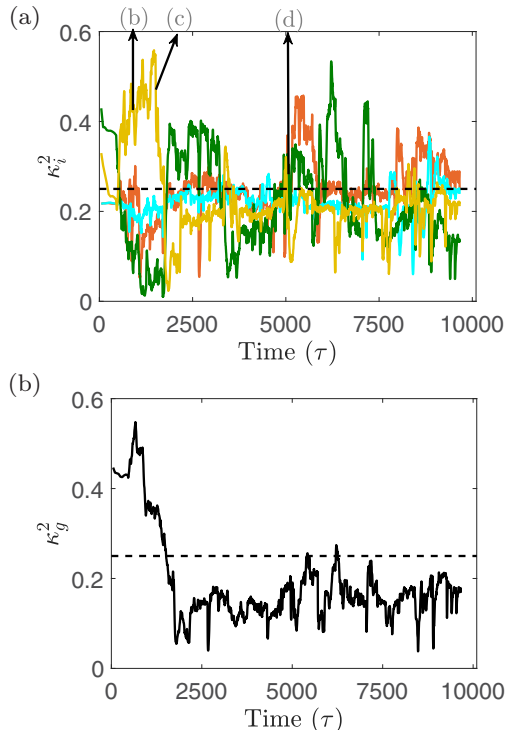


FIG. 7. (a) Shape anisotropy factor obtained from the eigenvalues of the individual chain gyration tensors. The labels at the top of the plot correspond to the times of the snapshots in Fig. 6. (b) Global shape anisotropy obtained from the eigenvalues of the global gyration tensor. The dotted black line corresponds to a ringlike topology at $\kappa^2 = 0.25$.

in Fig. 6(a). Within 880τ , Fig. 6(b) and Fig. 7(a) show that the coiled chain undergoes massive rearrangements, whereas the ring chains remain intact. We call this step “splaying,” where the chains freely “search” for nearby chains by random segmental motion. The time scales of rapid conformational fluctuations in this multichain system are similar to those for a single MC chain in solution reported by Li *et al.* [19]. One of the coiled chains (represented in green color) undergoes conformational fluctuations and wraps around the two ring chains, bringing the two ring chains together [Fig. 6(c)]. We call this step “engulfing,” which involves a chain “grabbing” nearby chains. This action arises from the strong intermolecular interaction. As a consequence, the ring chains change their orientation (represented in orange and cyan colors) from having their ring planes parallel to each other to being at an angle.

Subsequent to the engulfment step, the chains which are together at that point (green, orange, and cyan) rearrange to form the single fibrillar structure in Fig. 6(c); their ring axes are almost parallel to each other, with the formerly coiled green chain now adopting a toroidal conformation. The randomly coiled yellow chain continues to undergo rearrangement by splaying in a seemingly random fashion in the time period between snapshots Figs. 6(b) and 6(c), as indicated by the fluctuations in its shape anisotropy in Fig. 7(a). The aforementioned rapid conformational fluctuations and the engulfing steps for the green chain repeat for the yellow chain in Fig. 6(d), to form ultimately a fibrillar structure with four rings.

Interestingly, those chains which were initialized in a ringlike structure also undergo structural changes, as exemplified by the spike in the shape anisotropy factor of the chain displayed in orange color at point (d) in Fig. 7(a). These fluctuations are analogous to what we previously observed for the jammed initial configuration in Fig. 3, indicating that the ring-shaped structure formed from an initial system of relaxed and ring chains is also metastable. This result is again at odds with a mechanism wherein rings stack to form fibrils. Further, even after different chains collapse into a single structure, the shape anisotropies of all the ring chains fluctuate about their mean positions, as seen by the fluctuations in κ_i^2 [Fig. 7(a)] between 6000 and 8000τ . Such fluctuations can act as further sites for engulfing in a system containing even more than four chains.

To examine the overall structure of the multichain system, Fig. 7(b) displays the global shape anisotropy factor κ_g^2 . Initially, since the system has some chains which are randomly oriented, κ_g^2 starts at a random initial value, which may or may not be near the ringlike value of 0.25 . Over time, the system settles around $\kappa_g^2 = 0.18$. Notably, the system does not

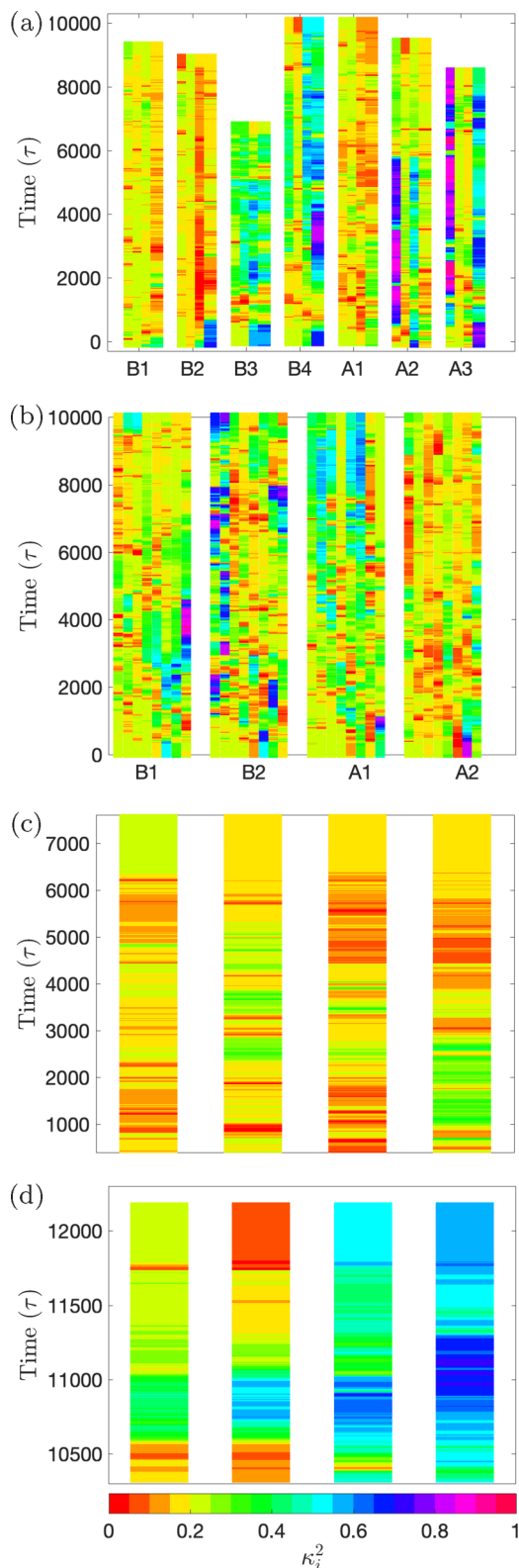


FIG. 8. Evolution of the shape anisotropy factor for (a) four-chain systems and (b) eight-chain systems. Each block of data corresponds to a single simulation. Simulations initiated in block configuration start with label B and those in alternating configuration start with label A. In each simulation, the first two (for four-chains) or four (for eight-chains) color maps from the left correspond to chains initiated in a ring configuration, and the others correspond to chains initiated in random coil configuration. (c) Zoomed version

possess a perfect ring structure ($\kappa_i^2 = 0.25$) indicating that the final fibril has structural defects. These observations from the shape anisotropy factor quantify the qualitative information obtained from the snapshot in Fig. 6(d) wherein some of the chains do not form a perfect stacked structure.

C. Generality of conformational fluctuations in methylcellulose systems

The results thus far make it clear that conformational fluctuations play a significant role in fibril formation. In this section we examine whether these conformational fluctuations occur irrespective of the initial configuration and the number of chains in the system. To this end, we consider results obtained from four-chain and eight-chain systems that are initialized in either block or alternating configurations.

To convey the information on conformational fluctuations from a large number of simulations in a compact way, Fig. 8 provides a color map of the shape anisotropy factor κ_i^2 of each chain as a function of time. The ringlike value of $\kappa_i^2 = 0.25$ corresponds to a yellowish-green shade. Each block of data corresponds to one simulation, with the left half of the data block corresponding to chains initiated in ring configuration and the right half corresponding to chains initiated in a coiled configuration. The systems initiated in block configuration have labels beginning with B and those in alternating configuration have labels beginning with A.

A general trend can be observed from Fig. 8(a). On the one hand, the chains that are initialized with random coil configurations, and thus start at a larger value of shape anisotropy factor ($\kappa_i^2 \geq 0.4$), first undergo frequent conformational fluctuations (splaying) before gradually settling to a value between 0.05 and 0.45. On the other hand, the chains that are initialized in the ringlike configurations ($\kappa_i^2 \approx 0.25$) remain in the range of 0.15 to 0.3 with occasional fluctuations to a value below 0.1 (bright red) and above 0.3 (pale to bright green), but the magnitude of these fluctuations is suppressed somewhat relative to the chains that were initialized as random coils. Figure 8 shows that irrespective of the initial configuration and the distance between the chains, all of the chains undergo conformational fluctuations. Further, we observe that the time scale for the large scale fluctuations near the start of the simulation in each case is $O(10^3\tau)$, similar to the value in Sec. III B, showing that the time scales of fluctuations are independent of the initial arrangement of the system.

In most of the cases studied, not only can the chains initiated in a random coil configuration splay, but the chains initialized in ringlike structure can also splay, and the order in which the chains splay is seemingly at random. For instance, Fig. 9(a) displays such an instance where all the chains undergo conformational fluctuations. For a clearer quantitative depiction, κ_i^2 values for data set A1 in Fig. 8(a) are shown in closeup in Fig. 8(c). After about 2000τ , at least one of the ringlike chains undergoes conformational fluctuations, as seen by the red (less than 0.15) and pale green (greater than

← of A1 in (a); (d) zoomed version of B4 in (a). Representative movies pertaining to the time evolution of all the simulations can be found in [32].

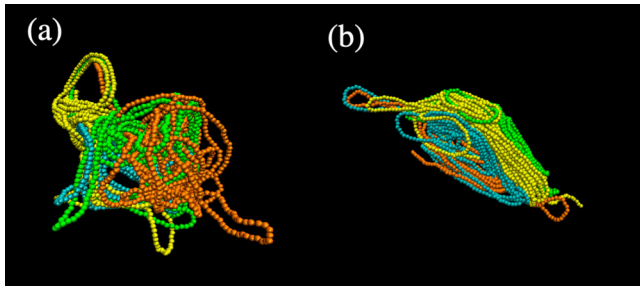


FIG. 9. (a) Snapshot showing splaying of all chains for case B4 at 2655τ . (b) Snapshot of the intermediate bundled structure at $11\,240\tau$. Other relevant snapshots for (b) are shown in Fig. S5 [32]. For both cases, orange and cyan colored chains were initiated in a ringlike configuration, whereas the other two chains were initiated in a random coil configuration.

0.35) regions in Figs. 8(a) and 8(c). These changes indicate that the ringlike chains within the fibril-like superstructure can act as further nucleating sites. Further, these fluctuations suggest that the ringlike structures may not be the equilibrium stable structure, at odds with the stacking mechanism but consistent with the results presented in Sec. III A. However, the fluctuation frequency is higher in those chains which are initiated in randomly coiled structure than those which are initiated in ring configurations.

In some cases (for example, cases B3 and B4 between $6 \times 10^3\tau$ and $1.2 \times 10^4\tau$), the κ_i^2 values for all of the chains vary between 0.50 and 0.60. Figure 9(b) displays such an instance where all chains are in a bundled structure. Unlike the splaying and engulfing steps, bundling is not observed for all simulations. Figure 8(d), a zoomed version of case B4 in Fig. 8(a), displays values between 0.50 and 0.60 for all chains around $11\,000\tau$. Although infrequent, a bundled configuration is also observed as an intermediate metastable state or at the end of some of our simulations. The global shape anisotropy factor for those systems which yielded a single structure at the end of our simulation is between 0.08 and 0.32; the final fibrillar structure for these four chain simulations does not possess a perfect ring structure, consistent with simulations of dilute two-chain systems.

Most cases which are initialized with four chains and within the minimum capture radius form a single fibril-like structure. However, some of our simulations produced two independent ringlike structures (one compound structure with three chains and the other with a single chain) within the time scale of the simulation (Fig. S6 [32]). This arises from the randomness of the conformational fluctuations or the absence of other chains during such fluctuations.

Figure 8(b) displays the color map for the shape anisotropy factor for systems consisting of eight chains. The qualitative results for eight-chain systems are similar to those of a four-chain system. The key difference is that the probability of forming multiple complex structures is higher in the case

of eight-chain systems compared to that of the four-chain systems. This arises from the slow diffusion of the complexes after a few chains merge.

In all of the systems studied here, we have kept the molecular weight fixed, and kept the initial ratio between the number of chains in a ring configuration and in a random chain configuration at 1:1. Although the simulations show that chains in a ring conformation can nucleate a fibril, they do not provide an estimate for the number of rings, their molecular weights, or the energy barrier required for nucleation to proceed. Simulations at these concentrations with only one ring and the remainder of the chains in a random coil form either globules [30] or a group of parallel chains. A systematic study with different ratio of ring to random chain conformations at various molecular weights is necessary to understand the nucleation mechanism in detail, and represent an attractive option for future study.

IV. SUMMARY AND OUTLOOK

In this work, we utilized coarse-grained molecular dynamics simulation of multichain methylcellulose systems to understand the precursor mechanism of fibril formation. We confirmed that a ring stacking mechanism [30] produces the expected fibril precursor structure when the chains are initially in close proximity and collapsed into isolated rings. For simulations mimicking dilute MC solutions, however, we see that different precursor steps, including rapid conformational fluctuations and “engulfing” of nearby chains, act as precursor steps for fibril formation. Taken together, our simulations showed that the mechanism of fibril formation is distance dependent. Investigations of closely packed fibril structures showed that the fibril structure itself undergoes conformational fluctuations and provide evidence for a mechanism that could produce branching of fibrils. Systems comprised of both toroidal chains and randomly coiled chains also indicated the importance of conformational fluctuations and engulfing steps in fibril formation. For some of these simulations, the chains collapsed into a bundled structure. Inasmuch as our simulations produce fibril-like structures without the need to initially collapse all of the chains into rings, they support a nucleation mechanism rather than the ring stacking mechanism [30].

ACKNOWLEDGMENTS

V.S. acknowledges fruitful discussions with Dr. Xiaolan Li during the initial stages of this work. This work was supported primarily by the National Science Foundation through the University of Minnesota Materials Science Research and Engineering Center under Award No. DMR-1420013. The authors acknowledge the Minnesota Supercomputing Institute (MSI) at the University of Minnesota for providing resources that contributed to the research results reported within this paper.

[1] J. R. Lott, J. W. McAllister, M. Wasbrough, R. L. Sammler, F. S. Bates, and T. P. Lodge, Fibrillar structure in aqueous

methylcellulose solutions and gels, *Macromolecules* **46**, 9760 (2013).

- [2] J. W. McAllister, P. W. Schmidt, K. D. Dorfman, T. P. Lodge, and F. S. Bates, Thermodynamics of aqueous methylcellulose solutions, *Macromolecules* **48**, 7205 (2015).
- [3] J. W. McAllister, J. R. Lott, P. W. Schmidt, R. L. Sammler, F. S. Bates, and T. P. Lodge, Linear and nonlinear rheological behavior of fibrillar methylcellulose hydrogels, *ACS Macro Lett.* **4**, 538 (2015).
- [4] W. S. Denham and H. Woodhouse, CLXXXVI.-the methylation of cellulose, *J. Chem. Soc., Trans.* **103**, 1735 (1913).
- [5] L. Rebenfeld and E. Pacsu, Cellulose studies: Part XIX. distribution of methoxyl groups in partly methylated celluloses, *Text. Res. J.* **24**, 941 (1954).
- [6] E. Heymann, Studies on sol-gel transformations. I. The inverse sol-gel transformation of methylcellulose in water, *Trans. Faraday Soc.* **31**, 846 (1935).
- [7] K. Nishinari, K. E. Hofmann, H. Moritaka, K. Kohyama, and N. Nishinari, Gel-sol transition of methylcellulose, *Macromol. Chem. Phys.* **198**, 1217 (2003).
- [8] T. Kato, M. Yokoyama, and A. Takahashi, Melting temperatures of thermally reversible gels IV. Methyl cellulose-water gels, *Colloid Polym. Sci.* **256**, 15 (1978).
- [9] T. Ito, Y. Ishikawa, S. Okano, T. Hattori, R. Fujii, T. Shinozawa, and A. Shibuya, Cloning of human neuroblastoma cells in methylcellulose culture, *Cancer Res.* **47**, 4146 (1987).
- [10] P. Colombo, Swelling-controlled release in hydrogel matrices for oral route, *Adv. Drug Deliv. Rev.* **11**, 37 (1993).
- [11] V. H. Freedman and S. Shin, Cellular tumorigenicity in nude mice: Correlation with cell growth in semi-solid medium, *Cell* **3**, 355 (1974).
- [12] K. R. Kamath and K. Park, Biodegradable hydrogels in drug delivery, *Adv. Drug Deliv. Rev.* **11**, 59 (1993).
- [13] K. Arai and T. Shikata, Hydration/dehydration behavior of cellulose ethers in aqueous solution, *Macromolecules* **50**, 5920 (2017).
- [14] L. Li, H. Shan, C. Y. Yue, Y. C. Lam, K. C. Tam, and X. Hu, Thermally induced association and dissociation of methylcellulose in aqueous solutions, *Langmuir* **18**, 7291 (2002).
- [15] Y. Xu, C. Wang, K. C. Tam, and L. Li, Salt-assisted and salt-suppressed sol-gel transitions of methylcellulose in water, *Langmuir* **20**, 646 (2004).
- [16] R. Bodvik, L. Karlson, K. Edwards, J. Eriksson, E. Thormann, and P. M. Claesson, Aggregation of modified celluloses in aqueous solution: Transition from methylcellulose to hydroxypropylmethylcellulose solution properties induced by a low-molecular-weight oxyethylene additive, *Langmuir* **28**, 13562 (2012).
- [17] J. P. A. Fairclough, H. Yu, O. Kelly, A. J. Ryan, R. L. Sammler, and M. Radler, Interplay between gelation and phase separation in aqueous solutions of methylcellulose and hydroxypropylmethylcellulose, *Langmuir* **28**, 10551 (2012).
- [18] W. Huang, R. Ramesh, P. K. Jha, and R. G. Larson, A systematic coarse-grained model for methylcellulose polymers: Spontaneous ring formation at elevated temperature, *Macromolecules* **49**, 1490 (2016).
- [19] X. Li, F. S. Bates, and K. D. Dorfman, Rapid conformational fluctuations in a model of methylcellulose, *Phys. Rev. Materials* **1**, 025604 (2017).
- [20] F. Vargas-Lara and J. F. Douglas, Fiber network formation in semi-flexible polymer solutions: An exploratory computational study, *Gels* **4** (2018).
- [21] D. M. Hall, I. R. Bruss, J. R. Barone, and G. M. Grason, Morphology selection via geometric frustration in chiral filament bundles, *Nat. Mater.* **15**, 727 (2016).
- [22] I. R. Bruss and G. M. Grason, Non-Euclidean geometry of twisted filament bundle packing, *Proc. Natl. Acad. Sci. USA* **109**, 10781 (2012).
- [23] G. M. Grason, Defects in crystalline packings of twisted filament bundles. I. Continuum theory of disclinations, *Phys. Rev. E* **85**, 031603 (2012).
- [24] W. Huang, M. Huang, Q. Lei, and R. G. Larson, A simple analytical model for predicting the collapsed state of self-attractive semiflexible polymers, *Polymers* **8**, 264 (2016).
- [25] Y. Rotbaum, G. Parvari, Y. Eichen, and D. Rittel, Static and dynamic large strain properties of methyl cellulose hydrogels, *Macromolecules* **50**, 4817 (2017).
- [26] P. W. Schmidt, S. Morozova, P. M. Owens, R. Adden, Y. Li, F. S. Bates, and T. P. Lodge, Molecular weight dependence of methylcellulose fibrillar networks, *Macromolecules* **51**, 7767 (2018).
- [27] M. Jaspers, A. C. H. Pape, I. K. Voets, A. E. Rowan, G. Portale, and P. H. J. Kouwer, Bundle formation in biomimetic hydrogels, *Biomacromolecules* **17**, 2642 (2016).
- [28] T. P. Lodge, A. L. Maxwell, J. R. Lott, P. W. Schmidt, J. W. McAllister, S. Morozova, F. S. Bates, Y. Li, and R. L. Sammler, Gelation, phase separation, and fibril formation in aqueous hydroxypropylmethylcellulose solutions, *Biomacromolecules* **19**, 816 (2018).
- [29] M. Kong, I. Saha Dalal, G. Li, and R. G. Larson, Systematic coarse-graining of the dynamics of self-attractive semiflexible polymers, *Macromolecules* **47**, 1494 (2014).
- [30] V. V. Ginzburg, R. L. Sammler, W. Huang, and R. G. Larson, Anisotropic self-assembly and gelation in aqueous methylcellulose-theory and modeling, *J. Polym. Sci. B* **54**, 1624 (2016).
- [31] S. Plimpton, Fast parallel algorithms for short-range molecular dynamics, *J. Comput. Phys.* **117**, 1 (1995).
- [32] See Supplemental Material at <http://link.aps.org/supplemental/10.1103/PhysRevMaterials.3.055601> for (i) simulation methodology, (ii) algorithms for generating initial configurations and corresponding MATLAB codes, (iii) diffusion calculation, (iv) supplemental figures, (v) movies pertaining to Fig. 8, and (vi) URL for LAMMPS codes, postprocessing codes, and movie files.
- [33] M. P. Allen and D. J. Tildesley, *Computer Simulation of Liquids* (Clarendon Press, New York, 1989).
- [34] D. N. Theodorou and U. W. Suter, Shape of unperturbed linear polymers: Polypropylene, *Macromolecules* **18**, 1206 (1985).
- [35] C. Keary, Characterization of methocel cellulose ethers by aqueous sec with multiple detectors, *Carbohydr. Polym.* **45**, 293 (2001).